Use of Sol–Gels as Solid Matrixes for Simultaneous Multielement Determination by Radio Frequency Glow Discharge Optical Emission Spectrometry: Determinations of Suspended Particula...

ARTICLE *in* ANALYTICAL CHEMISTRY · JUNE 2003

Impact Factor: 5.64 · DOI: 10.1021/ac020673v · Source: PubMed

Anal. Chem. **2003,** *75,* 2243−2250

Use of Sol−Gels as Solid Matrixes for Simultaneous Multielement Determination by Radio Frequency Glow Discharge Optical Emission Spectrometry: Determinations of Suspended Particulate Matter

W. Clay Davis,[†] Brad C. Knippel,[†] Julia E. Cooper,[‡] Bryan K. Spraul,[†] Jeanette K. Rice,[§] Dennis W. Smith, Jr.,[†] and R. Kenneth Marcus*[,†]

Department of Chemistry, Howard L. Hunter Laboratory, Clemson University, Clemson, South Carolina 29634, Department of Chemistry, Daniel-Moultrie Science Center, Erskine College, Due West, South Carolina 29639, and Department of Chemistry, Herty Building, Georgia Southern University, Statesboro, Georgia 30460

A new approach for the analysis of particulate matter by radio frequency glow discharge optical emission spectrometry (rf-GD-OES) is described. Dispersion of the particles in a sol−gel sample matrix provides a convenient means of generating a thin film suitable for sputter-sampling into the discharge. Acid-catalyzed sol−gel glasses synthesized from tetramethyl orthosilicate were prepared and spun-cast on glass substrates. The resultant thin films on glass substrates were analyzed to determine the discharge operating conditions and resultant sputtering characteristics while a number of optical emission lines of the film components were monitored. Slurries of powdered standard reference materials NIST SRM 1884a (Portland Cement) and NIST SRM 2690 (Coal Fly Ash) dispersed in the sols were cast into films in the same manner. Use of the sol−gels as sample matrixes allows for background subtraction through the use of analytical blanks and may facilitate the generation of calibration curves via readily synthesized, matrix-matched analytical standards in solids analysis. Detection limits were determined for minor elements via the RSDB method to be in the range of 1−10 μg/g in Portland Cement and Coal Fly Ash samples for the elements Al, Fe, Mg, S, and Si. Values for Ca were in the range of 15−35 μg/g. This preliminary study demonstrates the possibility of incorporating various insoluble species, including ceramics and geological specimens in powder form, into a solid matrix for further analysis by either rf-GD-OES or MS.

One of the large remaining challenges in the area of elemental analysis is the development of suitable methodologies for the direct solids multielement analyses of solid specimens that are by all accounts difficult to analyze in their native states. While there are a number of straightforward methods for readily placing most metallic samples into solution, inorganic solids (most typically oxides) present a plethora of problems toward achieving the end of being able to utilize methods of analysis that are based on solution nebulization for sample introduction. Examples of the sorts of materials that are encountered in this vein are geological materials, glasses and cements, and particulate matter of various forms. Rather than having to devise specific dissolution strategies, it is obvious that the development of methods that do not involve chemical modification of the sample matrix itself would be most beneficial.

Many popular direct solid sampling techniques, including laser ablation,[1−3] spark ablation (SA),[4,5] and direct current glow discharge (dc-GD) spectrometries[6−8] and X-ray fluorescence (XRF),[9−11] have been employed for direct solids multielement analysis. However, both SA and dc-GD methods require the sample to be electrically conductive in order for the respective discharge currents to flow. Modification of a nonconductive sample involves crushing the sample into powder form, subsequent mixing with a conductive binder (high-purity copper or silver powder), and compaction into a suitable shape.[12] The sample-to-conductive

* To whom correspondence should be addressed. E-mail: marusr@clemson.edu.

[†] Clemson University.

[‡] Erskine College.

[§] Georgia Southern University.

(1) Gunther, D.; Horn, I.; Hattendorf, B. *Fresenius J. Anal. Chem.* **2000**, *368*, 4−14.
(2) Russo, R. E.; Mao, X. L.; Gonzalez, J. J.; Mao, S. S. *J. Anal. At. Spectrom.* **2002**, *17*, 1072−1075.
(3) Guillong, M.; Gunther, D. *J. Anal. At. Spectrom.* **2002**, *17*, 831−837.
(4) Brenner, I. B.; Zander, A.; Kim, S.; Holloway, C. *Spectrochim. Acta, Part B* **1995**, *50*, 565−582.
(5) Coedo, A. G.; Dorado, T.; Padilla, I.; Fernandez, B. J. *Appl. Spectrosc.* **2000**, *54*, 1032−1039.
(6) Broekaert, J. A. C.; Lathen, C.; Brandt, R.; Pilger, C.; Pollmann, D.; Tschopel, P.; Tolg, G. *Fresenius J. Anal. Chem.* **1994**, *349*, 20−25.
(7) De Gendt, S.; Schelles, W.; Van Grieken, R.; Muller, V. *J. Anal. At. Spectrom.* **1995**, *10*, 681−687.
(8) Winchester, M. R.; Hayes, S. M.; Marcus, R. K. *Spectrochim. Acta, Part B* **1991**, *46*, 615−627.
(9) Revenko, A. G. *X-ray Spectrom.* **2002**, *31*, 264−273.
(10) Thomsen, V. B. E.; Schatzlein, D. *Adv. Mater. Processes* **2002**, *160*, 41−43.
(11) Evans, J. R.; Sellers, G. A.; Johnson, R. G.; Vivit, D. V.; Kent, J. *U.S. Geolog. Surv. Bull. 2144* **1997**.
(12) Caroli, S.; Senofonte, O.; Tamba, M. G. D.; Cilia, M.; Brenner, I. B.; Dvorochek, M. *Spectrochim. Acta, Part B* **1993**, *48*, 877−891.

10.1021/ac020673v CCC: $25.00
Published on Web 04/19/2003

binder ratio in the mixture can vary between 1:1 and 1:20, depending on the sample type.[7,8,12] Laser ablation with subsequent ICP-optical emission spectrometry (OES)/MS is quite suitable for direct analysis of conducting and nonconducting samples, eliminating time-consuming sample preparation procedures.[1] However, the ablation behavior is highly dependent on the samples' physical and chemical matrix.[3] Analysis by XRF, on the other hand, is nondestructive and allows direct analysis involving little or no sample preparation. Technological advances in instrumentation allow analysis of virtually all types of materials, including spatially resolved analysis on the micrometer level.[10,13] However, the method is insensitive for low-atomic number (Z) elements, is affected by the matrix absorption of the analyte fluorescence radiation, and has limited overall elemental power of detection. Dissolution of oxide materials in Li−glass fusions greatly simplifies matrix effects and provides a fairly universal preparation procedure for XRF analysis.[11,14]

Radio frequency (rf)-powered glow discharges have broadened the application for GD techniques because of their ability to directly atomize and analyze both conductive and nonconductive solid sample types.[15] The majority of research conducted in rf-GD methods has been in the bulk analysis of materials by emission and mass spectrometries,[16−19] although there is a growing interest in the capability of the technique for surface analysis of coated and multilayered materials.[20,21] Expanding the scope of layered materials and the types of information provided by rf-GD-OES analysis, lead zirconate−titanate (PZT) thin films synthesized through sol−gel chemistry have been characterized for qualitative information of the relationship between processing conditions and the structure of the deposited films.[22]

Beyond the relatively straightforward analysis of nonconductive bulk materials and films, studies in this laboratory have investigated the possibilities of analyzing powder-form refractory materials. Clearly, the aforementioned methods involving mixture of oxide powders with metallic ones, and then pressing a nominally conductive sample, are viable approaches for rf-GD analyses, though not required. Pan and Marcus[23] described the direct compaction of glass reference materials in powder form for analysis by rf-GD-OES. Uniform powders can be pressed to form disks of sufficient integrity for stable plasma operation, providing limits of detection and analytical precision that are close to those seen for bulk materials. Unfortunately, issues of entrapped gases in the course of the pressing procedure and the variability in particle sizes and composition likely encountered in real-world samples will be complicating issues. To directly address these issues, fusion with lithium metaborate has been investigated as a relatively straightforward means of sample preparation.[24] Indeed, analysis of coal fly ash dispersed in a lithium metaborate glass was found to be much easier to implement than direct compaction. Analyte optical emission was observed to stabilize quickly (<1 min.) and remain so for up to 10 min. The principle limitation of the approach was the high analytical blanks of the fusion matrix, typically not a problem in XRF, but sufficiently high to be problematic for the more sensitive rf-GD-OES method.

In a further effort to develop reliable methods of sample preparation for rf-GD analysis of refractory materials, immobilization of powder specimens in oxide matrixes formed by the sol−gel process has been investigated. Room-temperature sol−gel processing involves the hydrolysis and condensation of either silica or metal alkoxide monomers to produce a colloidal suspension (sol) and gelation of the sol to form an inorganic glass (gel) network.[25] Sol−gel-derived glasses have a wide variety of applications in analytical chemistry in that they provide a simple means of entrapping a variety of soluble and insoluble species within a stable glass matrix. Optical sensors,[26−29] modified electrodes,[30,31] chromatographic stationary phases,[32,33] and solid-phase microextraction supports[34] have utilized sol−gel chemistry in many forms. The chemistry of the sol−gel process is able to produce inorganic glass networks from either silica or metal alkoxide monomer precursors while providing a means to vary many of the physical properties (porosity, transparency, hardness) of the glasses.[25,35]

Dispersion and immobilization of particulate matter in sol−gel matrixes have been investigated for a wide variety of applications. Various optical properties of doped particles in sol−gel glasses and thin films have been studied.[36−38] For example, nanoparticles of Au and Ag suspended in thin-films exhibit enhanced Raman scattering and give rise to third-order nonlinear optical susceptibility.[39] Extensive research in the area of catalysis utilizing nanoparticles entrapped in sol−gel matrixes has also been undertaken.[40−43] Schimpf and co-workers have demonstrated

(13) Schields, P. J.; Gibson, D. M.; Gibson, W. M.; Gao, N.; Huang, H. P.; Ponomarev, I. Y. *Powder Diffr.* **2002**, *17*, 70−80.
(14) Claisse, F. *Glass Disks and Solutions by Fusion in Borates for Users of Claisse Fluxers*, 2nd ed.; Spex CertiPrep, 1999.
(15) Marcus, R. K. *J. Anal. At. Spectrom.* **1994**, *9*, 1029−1037.
(16) Duckworth, D. C.; Marcus, R. K. *Anal. Chem.* **1989**, *61*, 1879−1886.
(17) Harville, T. R.; Marcus, R. K. *Anal. Chem.* **1993**, *65*, 3636−3643.
(18) Cho, W. B.; Woo, Y. A.; Kim, H. J.; Kim, I. J.; Kang, W. K. *Appl. Spectrosc.* **1997**, *51*, 1060−1066.
(19) Saprykin, A. I. *Ind. Lab.* **1999**, *65*, 83−94.
(20) Payling, R.; Jones, D. G.; Gower, S. A. *Surf. Interface Anal.* **1993**, *20*, 959−966.
(21) Marcus, R. K.; Anfone, A. B.; Luesaiwong, W.; Hill, T. A.; Perahia, D.; Shimizu, K. *Anal. Bioanal. Chem.* **2002**, *373*, 656−663.
(22) Marcus, R. K.; Schwartz, R. W. *Chem. Phys. Lett.* **2000**, *318*, 481−487.
(23) Pan, X. H.; Marcus, R. K. *Mikrochim. Acta* **1998**, *129*, 239−250.
(24) Luesaiwong, W.; Marcus, R. K. *Microchem. J.* **2003**, *74*, 59−73.
(25) Brinker, C. J.; Scherer, G. W. *Sol−gel Science: The Physics and Chemistry of Sol−gel Processing*; Academic Press: Boston, 1990.
(26) Skrdla, P. J.; Saavedra, S. S.; Armstrong, N. R.; Mendes, S. B.; Peyghambarian, N. *Anal. Chem.* **1999**, *71*, 1332−1337.
(27) Dunbar, R. A.; Jordan, J. D.; Bright, F. V. *Anal. Chem.* **1996**, *68*, 604−610.
(28) Xu, H.; Aylott, J. W.; Kopelman, R.; Miller, T. J.; Philbert, M. A. *Anal. Chem.* **2001**, *73*, 4124−4133.
(29) Cho, E. J.; Bright, F. V. *Anal. Chem.* **2002**, *74*, 1462−1466.
(30) Wang, J.; Pamidi, P. V. A.; Rogers, K. R. *Anal. Chem.* **1998**, *70*, 1171−1175.
(31) PetitDominguez, M. D.; Shen, H.; Heineman, W. R.; Seliskar, C. J. *Anal. Chem.* **1997**, *69*, 703−710.
(32) Wu, J. T.; Huang, P. Q.; Li, M. X.; Qian, M. G.; Lubman, D. M. *Anal. Chem.* **1997**, *69*, 320−326.
(33) Dulay, M. T.; Quirino, J. P.; Bennett, B. D.; Zare, R. N. *J. Sep. Sci.* **2002**, *25*, 3−9.
(34) Bigham, S.; Medlar, J.; Kabir, A.; Shende, C.; Alli, A.; Malik, A. *Anal. Chem.* **2002**, *74*, 752−761.
(35) Attia, S. M.; Wang, J.; Wu, G. M.; Shen, J.; Ma, J. H. *J. Mater. Sci. Technol.* **2002**, *18*, 211−218.
(36) Morita, M.; Rau, D.; Fujii, H.; Minami, Y.; Murakami, S.; Baba, M.; Yoshita, M.; Akiyama, H. *J. Lumin.* **2000**, *87*−*9*, 478−481.
(37) Yang, P.; Song, C. F.; Lu, M. K.; Yin, X.; Zhou, G. J.; Xu, D.; Yuan, D. R. *Chem. Phys. Lett.* **2001**, *345*, 429−434.
(38) Romano, S. D.; Acosta, E. O.; Durrschmidt, T.; Kurlat, D. H. *Colloids Surf., A* **2001**, *183*, 595−605.
(39) Ishizaka, T.; Muto, S.; Kurokawa, Y. *Opt. Commun.* **2001**, *190*, 385−389.
(40) Abu-Reziq, R.; Avnir, D.; Miloslavski, I.; Schumann, H.; Blum, J. *J. Mol. Catal., A* **2002**, *185*, 179−185.
(41) Xu, A. W.; Gao, Y.; Liu, H. Q. *J. Catal.* **2002**, *207*, 151−157.

partial hydrogenation of acrolein by gold nanoparticles supported in sol−gels,[43] while Abu-Reziq and co-workers have demonstrated hydrogenation and hydrogenolysis of various aromatic ketones with palladium nanoparticles and a soluble rhodium catalyst.[40]

We describe here preliminary results of an extension of previous works in the analysis of sol−gel prepared PZT thin films.[22] In this case, the sol−gel oxides based on tetramethyl orthosilicate (TMOS) are employed as a thin-film matrix for the analysis of refractory particulate matter by rf-GD-OES. Coal fly ash and Portland cement reference materials are added in slurry form to the sol mixture, though a good deal of optimization lies ahead. The sample preparation technique described here allows for the synthesis of solid undoped samples that can then be used as analytical blanks and the possibility of generating true matrix-matched calibration curves with prepared standards providing a new realm for solids analysis. Calibration curves could in principle be generated as well by doping of the TMOS solutions with either solid-form or aqueous standards. Aliquouts of the sol are spin-cast onto glass substrates for processing into oxide films ranging in thickness from ∼150 nm to 5 μm for the cases of the analytical blanks and the particle-doped films. RF-GD-OES analysis involves the exhaustive sputtering of the oxide films over the course of ∼3 min. while simultaneously monitoring the optical response of the analyte species. Optical micrographs illustrate the suspension of the particulate matter within the oxide films, and surface profilometry reveals the resultant sputtering characteristics. Limits of detection based on the RSDB approach are on the microgram per gram level based on the original bulk powders, equating to nanograms of material in the actual sputtered films. It is believed that this preliminary work suggests that the approach may have practical value following more detailed evaluation of the sample preparation procedures.

EXPERIMENTAL SECTION

Sol−Gel Film Preparation. Sol−gel stock solutions were prepared using microliter pipets by mixing 3908 μL of TMOS (Acros Organics), 1555 μL of methanol (Fisher Scientific, Pittsburgh, PA), 691 μL of water (Fisher Scientific), and 3.1 μL of 0.1 M HCl (Fisher Scientific) and allowed to stir for 1 h. The sol solution was split in half and 10 mg of the powdered standard reference materials of NIST SRM 1884a Portland Cement and NIST SRM 2690 Coal Fly Ash (Table 1) added to the sol−gel solutions to form slurries. Three applications (200 μL each) of the slurries were then spun-cast (Chemat Technology spin coater model KW-4a) onto (2.5 × 2.5 cm) glass microscope slides (Fisher Scientific) each for 40 s at 2000 rpm, resulting in an apparently dry (i.e., no residual solvent) film. The presence of residual solvent would have deleterious effects on the fundamental plasma processes and lead to severe instability. Once cast, the films were allowed to cure in a desiccator at room temperature until analysis on the same day of casting. At this point in the method development, it is clear that issues of particle size, composition, and homogeneity will likely be important in the analytical quality of this approach, but are beyond the scope of this basic demonstration of the methodology. The homogeneity of particles in the resultant oxide film (both areally and in depth) will also be a key issue to evaluate.

Table 1. Certified Values for NIST SRM 1884A Portland Cement and NIST SRM 2690 Coal Fly Ash

NIST SRM 1884a Portland Cement	mass fraction (%)	NIST SRM 2960 Coal Fly Ash	mass fraction (%)
Al_2O_3	4.264	Al	12.35
CaO	62.26	Ca	5.71
Cr_2O_3	0.0166	Mg	1.53
Fe_2O_3	2.695	Ti	0.52
K_2O	0.997	Fe	3.57
MgO	4.475	P	0.52
Mn_2O_3	0.0853	K	1.04
Na_2O	0.2161	Si	25.85
P_2O_5	0.1278	Na	0.24
SO_3	2.921	S	0.15
SiO_2	20.57		
SrO	0.2984		
TiO_2	0.186		

Instrumentation. A JY RF-5000 (Jobin-Yvon, Division of Instruments SA, Edison, NJ) optical spectrometer was employed for all analytical measurements. This instrument is a 0.5-m Paschen-Runge polychromator, which is presently outfitted with 26 optical channels, each sampled at a rate of 2 kHz.[44] The source optical emission is focused onto a 2400 gratings/mm ion-etched holographic grating via a MgF_2 plano-convex lens. The optical spectrometer is nitrogen purged, allowing for emission detection over a range of 110−620 nm with a practical resolution of ∼0.01 nm. Spectrometer control and data acquisition were accomplished by Jobin Yvon's Quantum 2000 ver. 1.1 software on a Hewlett-Packard Vectra VE computer. Data files were then exported, processed, and managed in the form of Microsoft (Seattle, WA) Excel files.

The discharge cell (anode) is constructed of stainless steel. A constant anode-to-cathode distance of 0.5 mm is ensured by a ceramic disk around the O-ring. A 4-mm-i.d. limiting orifice (anode) was employed for all of the described studies. The flat glass (microscope slide) sample support acting as the cathode is sealed against a PTFE O-ring by a pneaumatically controlled piston. A Dressler (Berlin, Germany) generator and matching network supplied 40 W of rf power to the back of the sample cathode. Discharge gas pressure in the GD source was monitored with a silicon diaphragm pressure transducer (model PX811-005 Omega, Stamford, CT) and a matching controller/meter (model DP41=S Omega). The pressure transducer allowed the absolute pressures of both Ar and He to be measured without bias at a resolution of ∼0.2 Torr.

The sputtered crater characteristics were obtained with a Tencor P-10 (Mountain View, CA) surface profilometer, employing a 12.5-μm diamond-tipped stylus. For this report, a 10-mm scan width including a collection of 5040 data points was employed, yielding a lateral resolution of 2.0 μm and a depth resolution of 25 Å.

Optical microscope images of the particle-doped sol−gels were taken with a Zeiss (Carl Zeiss MicroImaging, Inc., Thornwood, NY) Stemi 2000-c microscope equipped with a Spot Insight color

(42) Rath, A.; Aceves, E.; Mitome, J.; Liu, J.; Ozkan, U. S.; Shore, S. G. *J. Mol. Catal., A* **2001**, *165*, 103−111.

(43) Schimpf, S.; Lucas, M.; Mohr, C.; Rodemerck, U.; Bruckner, A.; Radnik, J.; Hofmeister, H.; Claus, P. *Catal. Today* **2002**, *72*, 63−78.

(44) Hartenstein, M. L.; Marcus, R. K. *J. Anal. At. Spectrom.* **1997**, *12*, 1027−1032.

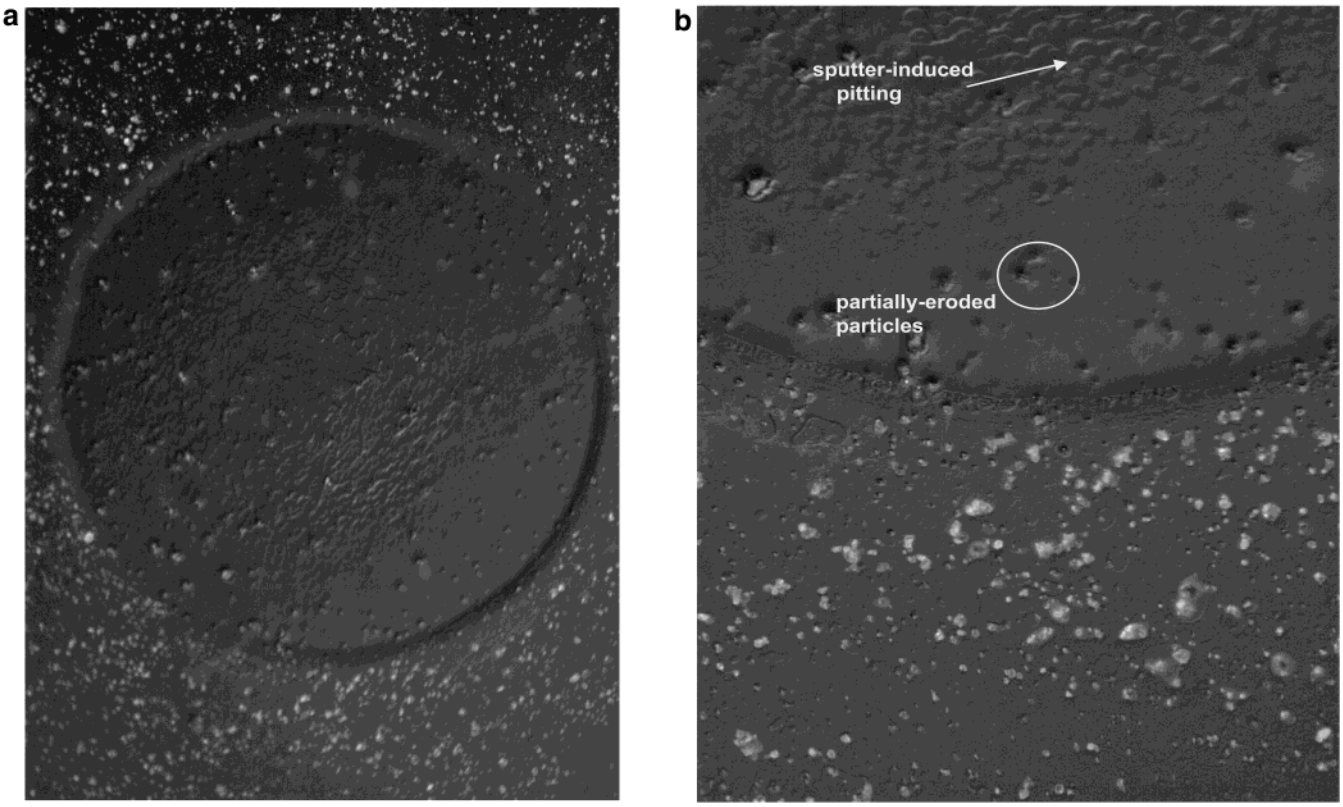

Figure 1. Optical microscope images of NIST SRM 1884a Portland Cement particles entrapped in a thin film sol−gel (a) 25× and (b) ∼200× after sputtering for a period of 10 min (rf power, 40 W; discharge gas, 1 Torr Ar/7 Torr He).

(model 3.2.0) CCD camera. A Dell Optiplex GX1 computer was employed for camera control and image acquisition by Spot Insight (Diagnostic Instruments Inc., Sterling Heights, MI) version 3.4 software. The Spot Insight CCD camera system consisted of an active image area of 11.8 × 8.9 mm with 1600 × 1200 (7.4 μm) pixels.

RESULTS AND DISCUSSION

At this point in the development of sol−gel sample preparation/rf-GD-OES analysis methodology, only the basic concept of utilizing sol−gels as a sample matrix for different particulates has been investigated. As such, a few specific attributes must be taken into consideration. In this work, successful incorporation of particulate matter in the gels is demonstrated. The sample preparation procedure is greatly simplified over the time-consuming pressed pellet method. The casting of reproducible thin films that have well-behaved sputtering characteristics is also an analytical requirement. The combined sample preparation and analysis program must provide sufficient sensitivity to solve practical problems. Ultimately, the ability to create calibration standards in a straightforward fashion is essential to performing meaningful quantitative analyses. As described in the following sections, it is believed that the fundamental traits observed to date suggest the use of sol−gels as an immobilization medium warrants more detailed development and evaluation.

Sputtering of Sol−Gel Prepared Oxide Films. The first requirement in any form of sample immobilization is the homogeneous distribution of sample components within the host matrix. Homogeneity in the present application is in the context of the distribution of the particles within the cast sol−gel film having a thickness of less than 10 μm and a plasma sampling area of 4 mm. Oxide films of this thickness are readily sputtered through to the substrate (termed exhaustive sputtering) in the rf-GD source in less than 5 min. As such, the distribution of particles in the *z*-direction (depth) is relatively unimportant. By the same token, the large sputtering area (in comparison to particle sizes) places fewer restrictions on the lateral distribution of suspended particles in comparison to laser or ion beam probing methods. The primary consideration in terms of distributing the particle-containing sol on the substrate is the ability to place a consistent amount of material in the sputtering area.

Optical micrographs are instructive in assessing the distribution of particles within the sol−gel film as well as fate of the sample following the analytical plasma cycle. Micrographs obtained following the sputtering of a film containing NIST SRM 1884a Portland Cement are presented in Figure 1. Figure 1a is a 25× magnification that clearly depicts the resultant sputtered crater formed in the film after sputtering for a period of 10 min at an rf power of 40 W. As will be shown in subsequent sections, this period of time is sufficient to penetrate the film and begin sputtering the glass substrate. Further magnification (∼200×) of the image shown in Figure 1b reveals clearly the immobilized particles in the native film on the exterior of the sputter crater. Also seen within the highlighted circle are remnants of particles that were not totally sputter-eroded within the crater. Based on a comparison between the sputtered and unsputtered regions, the vast majority of the particles originating within the sampling area

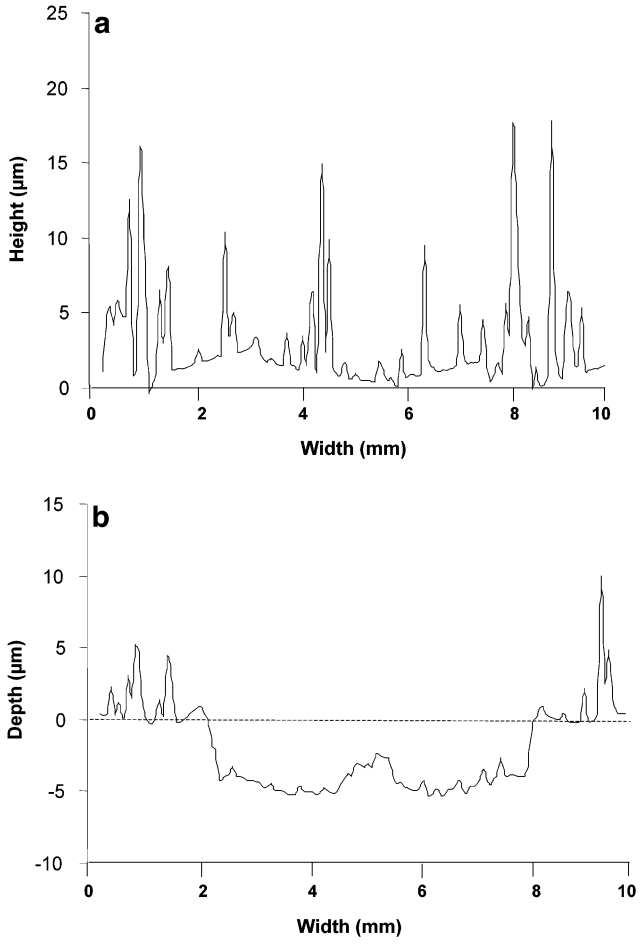

Figure 2. Diamond stylus profilometer tracings of the doped films (a) before and (b) after sputtering for a period of 10 min (rf power, 40 W; discharge gas, 1 Torr Ar/7 Torr He).

have been eroded away. In fact, the pitting in the upper portion of the figure is a direct consequence of the sputtering of the exposed substrate.

Just as optical micrographs provide information about the lateral dispersion of the cement particles in oxide film, diamond stylus profilometry allows assessment of the topography of the films and resultant sputtered craters. Figure 2a was obtained from the freshly cast sol−gel film containing cement particles. Seen across the profile are spikes of ∼5−15-μm height above the film surface. The tallest spikes reflect particles that are not fully imbedded in the oxide film, while shorter ones are representative of particles that are partially exposed. The apparent periodicity of the "baseline" is likely a remnant of ridging that may take place in the spinning of the sol−gel. The profilometry trace corresponding to a cross section of the sputtered crater of Figure 1 is displayed in Figure 2b. The central portion of the profile traces the sputtered crater having an average penetration depth of ∼5 μm beneath the original film surface. In comparison to topography outside of the crater (which still reflects particles on the film surface), the crater bottom is much smoother with no particle spikes. In fact, the observed convex crater shape (i.e., higher in the middle) is typical of those seen in GD depth profiling of materials when the source pressure is relatively high.[45] The form of the crater shape is a result of the potential distribution in the cathode dark space and redeposition of sputtered material.[46] This particular set of discharge operating conditions is not ideal for high-fidelity depth profiling but is likely suitable for the case where total analyte content in a film is desired from an exhaustive sputtering approach.

The most common matrix effect in all glow discharge methods is the result of the differences in sputtering rates between materials of different chemical composition and physical structure. For the case of the doped and undoped (blank) sol−gel films, the majority of the sample material is the formed oxide. Added particulate matter will contribute some composition differences but, more importantly, may lead to some morphological differences. For example, the blank sol−gel thin films sputtered at a rate of ∼2 nm/s across films of ∼135-nm average thickness. The sputter rates of the different particle-containing films were much faster, ∼25 and ∼12 nm/s for Portland cement and coal fly ash, respectively. These higher sputtering rates seem to compensate in some way for the increased thickness of these films; ∼5 and 2.3 μm, respectively, for the cement and fly ash-doped oxides. The fact that the cement (ground to pass a 75-μm sieve as reported on the assay) is more coarse than the coal fly ash (ground to pass 45-μm sieve as reported on the assay) would lead to the conclusion that the size of the doped particle has a dramatic effect on the resultant layer thickness, though the sputtering times are not as effected. (Actual particle size information was not reported on the NIST assays.) The higher sputtering rates seem to reflect the much lower densities (greater thickness for the same amount of material) of the doped films relative to the native oxides. Again, from the point of an exhaustive analysis where the total analyte signals are integrated over the course of the experiment, these differences in sputtering rates should be inconsequential.

It should be mentioned at this point that the actual discharge conditions employed in this study have not been optimized with regard to sputtering rates and excitation efficiencies. Previous rf-GD-OES analyses of glasses and nonconductive thin films have typically been performed in pure argon environments.[21,45,47] This was not the case for the sol−gels due to the higher sputtering rates of the sol−gels and their tendency to crack at high temperatures. In the case of argon plasmas operated at 40 W, which promotes an energetic plasma for excitation, stable analyte signals lasted for only a few seconds. More recent studies have shown that analytes within nonconductive sample can have greater emission intensity with a mixed discharge gas of Ar and He, even at slower sputtering rates.[48] Therefore, He was added to the Ar plasmas in order to slow the sputtering rates. As a compromise between analyte signal intensities and the desire to extend the sputtering time of the oxide films, the discharge gas employed here consisted of 1 Torr Ar and 7 Torr He. A detailed optimization of discharge parameters will be presented in a future report.

Analyte Emission Responses. The use of the simultaneous monitoring capabilities of a polychromator, as is typically applied in GD-OES depth profiling, is ideally suited for the sampling of optical emission from particles embedded in sol−gel matrixes.

(45) Parker, M.; Hartenstein, M. L.; Marcus, R. K. *Anal. Chem.* **1996**, *68*, 4213−4220.
(46) Bogaerts, A.; Gijbels, R. In *Glow Discharge Plasmas in Analytical Spectroscopy*; Marcus, R. K., Broekaert, J. A. C., Eds.; John Wiley and Sons: CHichester, U.K., 2003, pp 155−205.
(47) Anfone, A. B.; Marcus, R. K. *J. Anal. At. Spectrom.* **2001**, *16*, 506−513.
(48) Hartenstein, M. L.; Christopher, S. J.; Marcus, R. K. *J. Anal. At. Spectrom.* **1999**, *14*, 1039−1048.

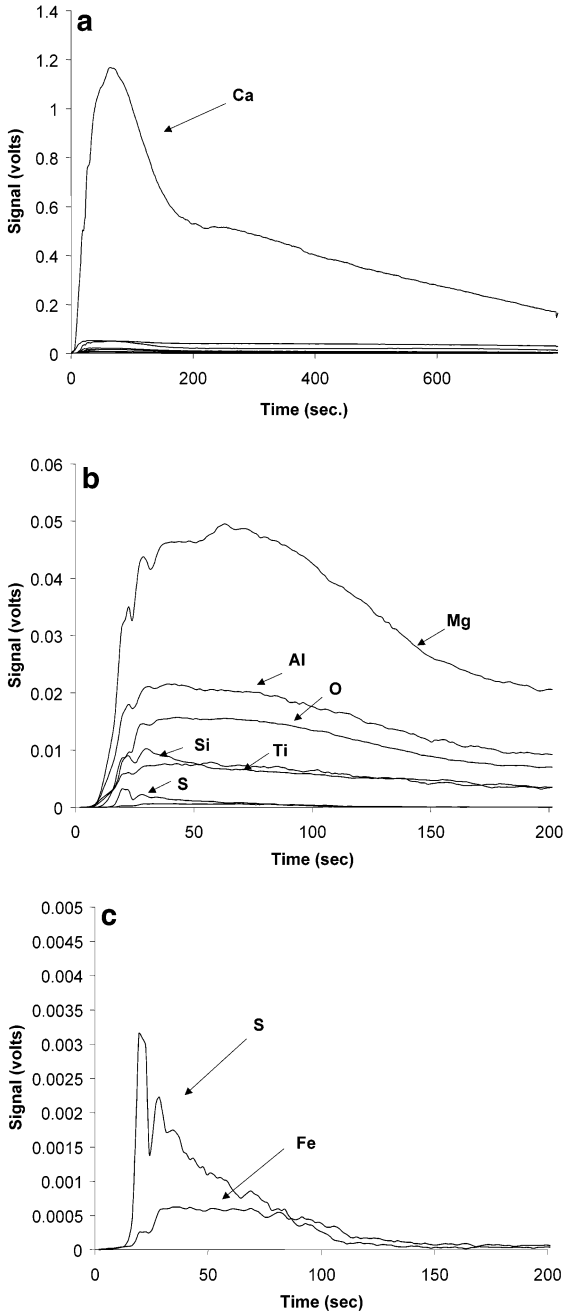

Figure 3. Depth profiles of sol−gel thin films doped with NIST SRM 1884a Portland Cement (rf power, 40 W; discharge gas, 1 Torr Ar/7 Torr He).

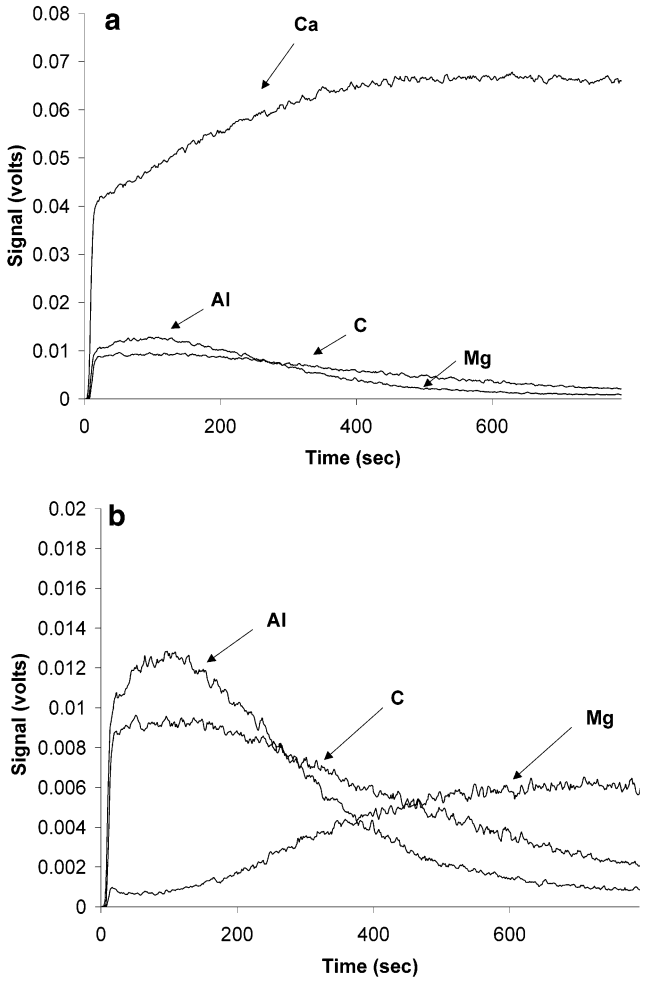

Figure 4. Depth profiles of sol−gel thin films doped with NIST SRM 2690 Coal Fly Ash (rf power, 40 W; discharge gas, 1 Torr Ar/7 Torr He).

The elemental depth profiles of the analytes from NIST 1884a Portland Cement particles entrapped oxide film are presented in Figure 3. On this particular scale, the Ca (I) emission is clearly seen as the most intense of all of the particle component elements. Of course, as listed in Table 1, $CaCO_3$ is the matrix compound in Portland cement. The temporal response for calcium is quite instructive in understanding sputtering through the sol−gel film. The Ca (I) response increases rapidly upon initiation of the plasma; the response passes through a maximum at ∼60 s. The intensity decreases steadily beyond this point, with a pronounced leveling after ∼200 s of sputtering. For the remainder of the 800-s sputtering cycle, the response drifts slowly downward, as the sputtering proceeds through the glass substrate, which of course contains appreciable amounts of Ca. Panels b and c of Figure 3 show the optical response for minor and trace species of the Portland cement particles for only the first 200 s of the burn as it is clear that this time frame encompasses the majority of the analyte responses in the film. The profiles demonstrate that rf-GD-OES can be used for analysis of both the primary and trace constituents of the particulates. In addition, emission from hard-to-excite nonmetal species in the cement, such as S, is also detected as seen in Figure 3c.

Glass slides provided a cost-effective substrate for these preliminary studies, although a substrate that provided an "analyte" optical response significantly different from that of the sol−gel samples would be ideal. Sol−gels cast onto metal substrates did not adhere to the metal surfaces and often cracked. Silicon wafers were also investigated as an alternative substrate. The wafers, as well as the glass, were cut into manageable sizes but are only able to be sputtered once. For this reason, the glass microscope slides provided a best means of producing a great number of samples for a relatively low cost.

As in the case of the Portland cement, the time required to sputter through the coal fly ash-doped sol−gel matrix to the glass substrate is ∼200 s. Figure 4 shows the emission profiles of sol−gel films containing the coal fly ash particles. Because the substrate contains significant amounts of Mg and Ca, the intensi-

Table 2. Integrated (200 s) Emission Intensities (I/Ar) for Various Elements in Undoped Sol−Gels, NIST SRM 1884A Portland Cement, and NIST SRM 2690 Coal Fly Ash[a]

element-transition (nm)	undoped sol−gel		Portland Cement		Coal Fly Ash	
	int ratio	% RSD	int ratio	% RSD	int ratio	% RSD
Al (I) 396.1	6.1×10^{-3}	8.3	1.3×10^{-1}	19	1.2×10^{-1}	17
C (I) 156.1	7.3×10^{-5}	9.2	8.6×10^{-5}	8.8	1.3×10^{-4}	7.9
Ca (II) 393.4	6.9×10^{-2}	3.1	6.6	20	5.2×10^{-1}	15
Cr (I) 425.4	5.0×10^{-2}	2.8	5.6×10^{-1}	6.9		
Fe (I) 371.9	5.4×10^{-4}	3.1	3.1×10^{-3}	33	2.7×10^{-4}	9.6
H (I) 122.6	1.5×10^{-1}	6.4	4.0×10^{-1}	7.5	2.6×10^{-1}	8.6
Mg (II) 280.3	2.6×10^{-2}	3.4	2.9×10^{-1}	12	1.4×10^{-2}	15
Mn (I) 258.6	6.8×10^{-4}	16	3.7×10^{-4}	16	3.0×10^{-3}	15
Ni (I) 341.5	2.8×10^{-5}	9.5			1.9×10^{-4}	8.2
O (I) 130.2	1.4×10^{-4}	6.3	9.8×10^{-2}	14	3.3×10^{-4}	6.6
P (I) 177.5	4.1×10^{-4}	7.1	1.3×10^{-4}	17	1.1×10^{-4}	16
S (I) 180.7	1.4×10^{-4}	17	2.0×10^{-3}	7.3	1.7×10^{-3}	9.1
Si (I) 288.2	2.4×10^{-4}	2.3	4.6×10^{-2}	22	1.9×10^{-3}	12
Ti (I) 365.3	4.4×10^{-4}	3.8	4.7×10^{-2}	15	2.1×10^{-3}	13
Zn (I) 213.9	4.4×10^{-4}	7.7			2.7×10^{-3}	14
Ar (I) 404.4		7.2		6.1		5.7

[a] Conditions: rf power, 40 W; discharge gas, 1 Torr Ar/7 Torr He.

ties of both species begin to increase while the Al intensity starts to decrease when the gel−substrate interface is reached. Clearly, if these elements were not present in the immobilized particles, they would not generate responses until the substrate was reached. The expanded scale of Figure 4b more clearly displays the ability to differentiate between the respective elements' content in the film and substrate. Of particular note is the C (I) response, which is reflective of remnant carbon content in the TMOS-derived matrix. The temporal profile is similar to that of the Al. Because carbon is a major component in all sol−gel films, and not to a large extent in the potential supports, it is envisioned that its response could be used as a generic end-point indicator and internal standard relative to the sputtering rate of the deposited film.

Table 2 is a compilation of the reproducibility obtained in the sample preparation, mounting, and analysis of doped and undoped sol gels. The emission data are reported as the integrated (200-s) emission intensities of the analyte transitions divided by that of the Ar (I) 404.4-nm response for the same time period. Previous studies in this laboratory have shown that the ratio of analyte responses to those of the discharge gas is a useful means of reducing sample-to-sample variations that are manifest in the plasma energetics (i.e., excitation conditions).[24,47] As depicted in Table 2, the sample-to-sample reproducibility (expressed as RSD) of the integrated emission intensities is generally better than 10% RSD for all of the target analytes for five replicate sol−gel castings of the spectroscopic blank (i.e., the undoped gel). This sets a baseline for the primary mixing and casting of the sol−gel and the reproducibility of the analytical conditions. The corresponding emission response (I/Ar) and precision data for quintuplet (n = 5) mixtures of the Portland cement and coal fly ash reference materials are also presented in Table 2. As expected, the ratios of the analyte element responses to the Ar (I) increase for the doped films. There is a lack of a correlation between the individual analyte intensities (ratios) and the individual element's precision.

Table 3. Detection Limits (μg/g) Using SBR-RSDB Approach for Various Elements in NIST SRM 1884a Portland Cement and NIST SRM 2690 Coal Fly Ash[a]

element-transition (nm)	Portland Cement	Coal Fly Ash
Al (I) 396.1	4.7	4.0
Ca (II) 393.4	14.7	34.9
Fe (I) 371.9	1.7	8.2
Mg (II) 280.3	0.8	8.0
S (I) 180.7	1.2	0.5
Si (I) 288.2	3.1	2.9

[a] Conditions: rf power, 40 W; discharge gas, 1 Torr Ar/7 Torr He.

It seems though that the highest degrees of imprecision correspond to the more refractory elements (e.g., Al, Fe, Ti, etc.). Interestingly, the relative precision between the two particle matrixes is the same even though there are definite differences in the particle sizes. At this preliminary stage of development, it is believed that the precision seen here suggests further promise as more regimented sample grinding, sizing, sol mixing, and casting procedures are developed.

Preliminary Limits of Detection. At this point in the development of the sol−gel sampling methodology, it is premature to undertake a detailed evaluation of all figures of merit. It is pertinent though to ascertain whether the method is likely to have sufficient sensitivity for practical analyses. In the absence of the generation of a comprehensive calibration function, limits of detection were generated using the relative standard deviation of the background (RSBD) method of calculation proposed by Boumans and Vrakking.[49] The RSDB method is a useful method of comparing the limits of detection between plasma sources and different spectrometer systems. In this method, the limit of detection is given by

$$\mathrm{LOD} = \frac{(0.01)3(\mathrm{RSDB})m}{(S/B)} \qquad (1)$$

where RSDB is the relative standard deviation in the background, S/B is the signal-to-background ratio, and m is the concentration of the analyte used in the determination (the cement and particulate matter here), with a value of 3 being used to give a >99% confidence level.The RSDB method can be applied in a few different ways; here we employ the average intensity value at the analyte transitions for the "blank" sol−gels as the background value (B). The RSDB value is the relative standard deviation for the five runs. The calculated limits of detection, based on the primary sample material, are presented for the cement and particulate matter matrixes in Table 3. As can be seen, the values here are generally on the single microgram per gram level. These values are consistent with others obtained in this laboratory by rf-GD-OES, including glass samples.[17,47] The singularly poor-performing element is calcium. This group has little experience with this element, but it is likely that the fact that the monitored transition is for the first ionic state (Ca (II)) and not well populated may explain the discrepancy. Based on the plasma energetics,

(49) Boumans, P. W. J. M.; Vrakking, J. J. A. M. *Spectrosc. Acta, Part B* **1987**, *42*, 819−840.

most transitions monitored by GD-OES systems are atomic in nature. It is believed that the values seen here bode well for continued development of this methodology. As a final note, it should be mentioned that, based on the amount of material deposited in the film and the sputtered area, the amount of material actually being sampled here is on the single-nanogram level.

CONCLUSIONS

Sol−gels have been applied in a wide variety of analytical applications from chemical-sensing platforms to chromatography stationary phases. Demonstrated here is the novel use of sol−gels as a sample matrix for analysis of particulate matter. These preliminary results suggest promise for the method for particulate analysis and also a number of optimization studies that must be performed. Extended sputtering times of the analyte-containing films were realized with the use of a Ar/He discharge gas mixture. Both primary and trace constituents of the particle samples have been detected by rf-GD-OES. The use of intensity ratios of the analyte species to those of the Ar discharge gas yield sample-to-sample precision of the order of 10% RSD. The primary sol−gel mixture can serve well as a spectroscopic blank as well as a dilution matrix for the preparation of analytical standards. Continuing studies will focus on optimization of the particle size of particulates, film homogeneity issues, and discharge source parameters to improve both the sputtering characteristics and quantification capabilities for species in particulates entrapped in sol−gel matrixes using both rf-GD-OES and rf-GD-TOFMS. Additionaly, the effect of sol−gel precursors and cross-linking of the sol−gel network on emission intensity will be of interest.

Received for review November 4, 2002. Accepted March 20, 2003.

AC020673V